Raman study of spin and orbital order and excitations in perovskite-type RVO_3 (R=La, Nd, and Y)

S. Miyasaka, J. Fujioka, and M. Iwama
Department of Applied Physics, University of Tokyo, Tokyo 113-8656, Japan

Y. Okimoto
Correlated Electron Research Center (CERC), National Institute of Advanced Industrial Science and Technology (AIST), Tsukuba 305-8562, Japan

Y. Tokura
Department of Applied Physics, University of Tokyo, Tokyo 113-8656, Japan; Spin Superstructure Project (SSS), ERATO, Japan Science and Technology Agency (JST), c/o AIST, Tsukuba 305-8562, Japan; and Correlated Electron Research Center (CERC), National Institute of Advanced Industrial Science and Technology (AIST), Tsukuba 305-8562, Japan

(Received 20 February 2006; published 27 June 2006)

The orders and excitations in spin and orbital sectors have been investigated for perovskite-type RVO_3 (R=La, Nd, and Y) by measurements of Raman scattering spectra. The orbital excitation bands emerge in the C-type spin- and G-type orbital-ordered phases commonly for the three RVO_3 compounds. The investigation of resonance effect on the Raman scattering spectra indicates the quasi-one-dimensional orbital excitation corresponding to the exchange of the occupied orbital state (yz or zx state) on the neighboring sites, to be termed a two-orbiton in analogy to two-magnon in antiferromagnetically ordered states. Among the three compounds, YVO_3 alone undergoes the phase transition from the C-type spin- and G-type orbital ordered state to G-type spin- and C-type orbital-ordered one, as temperature is lowered. In the lowest-temperature ordered phase, the Raman band assigned to two-magnon excitation is observed. In these compounds, structural distortions coupled with the respective orbital orders activate the specific Raman bands assigned to oxygen stretching modes. In the G-type orbital-ordered phase in YVO_3, the phonon mode shows a two-peak feature, while that in other compounds the single-peak one. This suggests that the nominally G-type orbital-ordered state in YVO_3 involves the short-range correlation or fluctuation of the orbital C-type, making this phase distinct from the prototypical G-type orbital ordered state as in $LaVO_3$ and $NdVO_3$.

DOI: 10.1103/PhysRevB.73.224436 PACS number(s): 71.27.+a, 71.70.Gm, 75.30.−m, 78.30.−j

I. INTRODUCTION

Transition-metal oxides with perovskite or related structures offer a source of intriguing physics, such as Mott transition,[1,2] high-temperature superconductivity,[3] and the colossal magnetoresistance (CMR).[4] Recent investigations on the CMR manganites have raised great interest in the interplay among spin, charge, orbital, and lattice degrees of freedom. Among them, the research on the orbital ordering and related phenomena has been accelerated by discovery of CMR in hole-doped perovskite-type manganese oxides, and orbital physics has become one of the most important topics in condensed matter physics.[5] Long range order of orbitals allows the orbital excitation as its dynamical disorder. The collective orbital excitation in the orbital-ordered state is termed the orbital wave or orbiton, in analogy to the spin wave or magnon in the magnetically ordered state. One such compound, where the orbiton has been observed, is $LaMnO_3$ with the ordering of e_g orbital.[6] In this system, the strong Jahn-Teller coupling suppresses the quantum fluctuation, and resultantly the orbital behaves semiclassically. Compared with the manganites, the perovskite-type vanadium oxide RVO_3 (R= rare-earth ion or Y), which shows the ordering of the t_{2g} orbital, is an ideal system to study the quantum dynamics of orbitals. This is because the Jahn-Teller coupling energy is much less in the t_{2g} electron systems than in the e_g ones.[7]

The vanadium oxide RVO_3 is a prototypical t_{2g} electron system with the close interplay between orbital and spin degrees of freedom. This system has a $Pbnm$ orthorhombic structure with lattice constants of $a \approx b \approx c/\sqrt{2}$ at room temperature. These compounds exhibit two kinds of spin- and orbital-ordered states depending on the R-site ions. Figure 1(a) reproduces a phase diagram of spin ordering (SO) and orbital ordering (OO) in this system.[8] The patterns of the SO and OO in this system are schematically shown in Figs. 1(b) and 1(c). All RVO_3 undergo a magnetic transition from paramagnetic to C-type antiferromagnetic and also a lattice-structural phase transition from orthorhombic to monoclinic lattice accompanied concomitantly with the G-type OO as temperature is lowered. Two electrons are present in the t_{2g} sector of V^{3+}. One electron always occupies d_{xy} orbital due to the symmetry-lowered crystal field by the orthorhombic distortion, which is coupled ferromagnetically (through Hund's-rule coupling) to the other electron in either d_{yz} or d_{zx} orbital forming a spin S=1. These spins are arranged ferromagnetically along the c axis and antiferromagnetically in the ab plane (spin C-type),[9–11] while the d_{yz}/d_{zx}-orbital order is alternating in all the orthogonal directions (orbital G-type).[12–14] As shown in Fig. 1(a), the C-type SO and

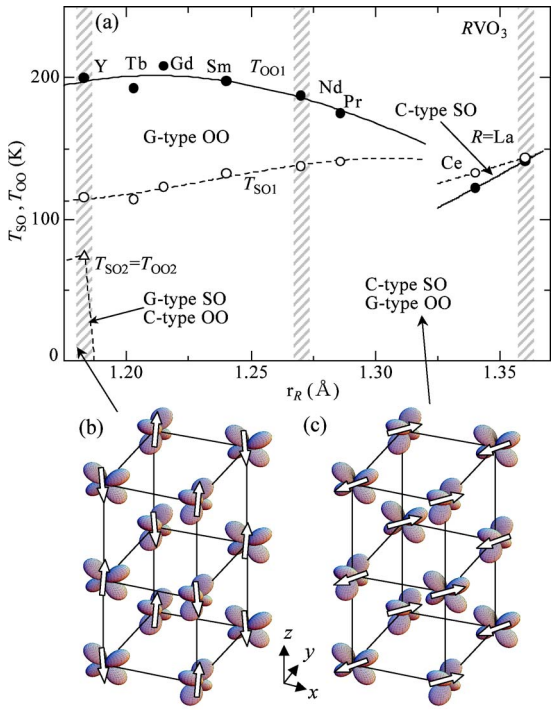

FIG. 1. (Color online) (a) Spin-orbital phase diagram of RVO_3 (R=Y-La) as reproduced from Ref. 8, where r_R on the abscissa is the R-site ionic radius. Closed and open circles, and open triangle indicate the transition temperatures of the G-type orbital ordering (OO) (T_{OO1}), the C-type spin ordering (SO) (T_{SO1}), and the G-type SO and C-type OO ($T_{SO2}=T_{OO2}$), respectively. (b), (c) The schematic structures of the G-type SO and C-type OO, and the C-type SO and G-type OO in RVO_3, respectively. Open arrows and lobes indicate spins, and occupied d_{yz} and d_{zx} orbitals on the vanadium ions, respectively. The commonly occupied d_{xy} orbitals are displaced for clarity.

G-type OO transition temperatures T_{SO1} and T_{OO1}, respectively, depend on the ionic radius of the R-site ion, which controls the degree of the tilting of VO_6 octahedra in distorted perovskite lattice.[8] The compounds with R=Lu to Pr undergo the orthorhombic-monoclinic structural phase transition concomitantly with the G-type OO at T_{OO1} ($>T_{SO1}$), indicating that the orbital correlation persists at high temperature without long-range magnetic ordering. As the ionic size of the R-site increases from Lu to La, the deviation of the V-O-V bond angle from 180 degrees as well as Jahn-Teller distortion of VO_6 octahedra gradually decreases. The increase of the V-O-V bond angle results in increase of transfer interaction and hence in enhancement of the spin and orbital exchange interactions between the nearest-neighbor V sites.[9,13,14] The T_{SO1} monotonously increases perhaps due to the increase of exchange interaction as the R-site is changed from Lu to Pr. With the increase of the R-site ionic radius, on the other hand, T_{OO1} reaches the maximum around R=Gd and decreases towards R=Pr. This is perhaps a result of the competition between the increase of the orbital exchange interaction and the suppression of the Jahn-Teller instability. For $CeVO_3$ and $LaVO_3$ with small orthorhombic lattice distortion, the C-type spin correlation appears to develop primarily and then induces the G-type OO. In RVO_3 with the large orthorhombic lattice distortion, by contrast, another SO and OO pattern shows up as the ground state; that is the G-type SO with the antiferromagnetic coupling between V^{3+} (S=1) spins in all the orthogonal directions and the C-type OO with the alternate $d^1_{xy}d^1_{yz}/d^1_{xy}d^1_{zx}$ electron configuration in the ab plane and the identical one along the c axis at the ground state. YVO_3, which shows a temperature-induced magnetization reversal phenomenon,[15] is located near the boundary between these two spin- and orbital-ordered phases in the phase diagram, and undergoes the subsequent magnetic transition from C type to G type with decreasing temperature.[8,10–13] Below the G-type SO transition temperature (T_{SO2}), the pattern of the OO concomitantly turns into C -type, accompanying the lattice-structural change due to the collective Jahn-Teller distortion.

In the RVO_3, the long-range SO provides an interesting laboratory for investigating the orbital dynamics. There are two reasons to treat the spin and the orbital unequally. One is that the spin has S=1, while the orbital pseudospin T=1/2 reflecting the two possible states d_{yz} and d_{zx}. This means that the quantum fluctuation of the orbital is stronger than that of the spin. The other reason is that the exchange interaction is three dimensional for spins, while it is quasi one dimensional for orbitals particularly in the C-type spin ordered phase in RVO_3. This is due to the destructive interference of various orbital exchange processes, as revealed by previous studies.[16–18] Therefore, the spin can be regarded as a classical variable forming a three-dimensional long-range order, providing a quasi-one-dimensional model for the orbital dynamics. This has recently been investigated in terms of a spin wave approximation for the orbital pseudospin.[19] Considering the one-dimensional (1D) nature of the quantum orbital dynamics more explicitly, the theoretical treatment based on the 1D fermion (pseudo-spinon) picture was adopted to describe the 1D-like orbital excitation by Miyasaka *et al.*[20] We report here a comprehensive experimental study on the Raman scattering spectra in this quasi-one-dimensional orbital system, i.e., in the C-type spin- and G-type orbital-ordered state. A part of results on this issue was already published.[20] Here, we take the same assignment of the orbital excitation bands as done in Ref. 20. In this paper, we report more detailed results of experimental study, not only for R=La and Nd but also for R=Y at temperatures in between $T_{OO2}=T_{SO2}$ and T_{SO1}. An appreciable variation of the Raman spectra in the spin C-type and orbital G-type state is noted with change of R=La/Nd to R=Y. As mentioned above, YVO_3 undergoes another SO and OO transition to the spin G-type and orbital C-type state. To clarify the lattice, spin, and orbital dynamics in this G-type spin- and C-type orbital-ordered state, we report results of Raman scattering spectra also for this low-temperature phase of YVO_3.

II. EXPERIMENTAL PROCEDURES

A. Sample preparation

Single crystals of RVO_3 (R=La, Nd, and Y) were grown by the floating zone method. Polycrystalline powder was first prepared by solid-state reaction using R_2O_3 and V_2O_5 as starting materials. The mixed powders of the starting mate-

rials were reacted at 600 and 1200 °C in flow of forming gas of Ar/H_2 (93/7%). The powders were pulverized again and sintered at 1350 °C in the same condition. Then the powders were pressed into a rod (~5 mmϕ×100 mm) and sintered at 1500 °C for 10 h in flow of forming gas of Ar/H_2. The crystal growth was performed on this sintered rod using a halogen-lamp image furnace at a rate of 20–30 mm/h under an atmosphere of pure Ar. The obtained crystals were pulverized and checked by powder x-ray diffraction with Cu $K\alpha$ radiation. The cation ratio of the growth crystals was also checked by the inductively coupled plasma atomic emission spectroscopy. The grown crystals of RVO_3 were confirmed to be detwinned between the *ac* and *bc* planes by Laue reflection and single-crystal x-ray diffraction with a four-circle diffractometer. The single crystals were oriented with use of Laue-diffraction patterns, and cut into plates with the $(a+b)c$ and *ab* surfaces. The surfaces of the RVO_3 crystals were polished to optical flatness with alumina powder. To remove the mechanical stress induced by surface-polishing, we annealed the crystals at 1000 °C for 24 h in flow of forming gas of Ar/H_2 (93/7%).

B. Raman scattering measurements

In the measurements of polarized Raman spectra, light (0.5 mW) from a He-Ne laser (1.96 eV) or from an Ar ion laser (2.41 or 2.71 eV) was focused onto a spot in 0.01 mm diameter on the sample surface. For the present study, we employed the backscattering configuration. The scattering light was dispersed by a triple monochromator and detected with a liquid-nitrogen-cooled charge-coupled device (CCD) detector. The spectral intensities were calibrated to the instrumental sensitivity and corrected by the absorption coefficient and reflectivity of the incident and scattered lights, which were derived from optical reflectivity data. Polarized geometry is described using the conventional notation $k_i(e_i\ e_s)k_s$, where k_i and e_i represent the propagation direction and the polarization of the incident light, respectively, and k_s and e_s those of the scattered light. Optical axes, *x*, *y*, and *z* are taken parallel to the orthorhombic crystal axes, $a+b$, $a-b$, and *c*, and hence nearly to the directions of V-O-V bonds.

III. *C*-TYPE SPIN- AND *G*-TYPE ORBITAL-ORDERED PHASE

In this section, we represent the experimental results in the *C*-type spin- and *G*-type orbital-ordered phase, and discuss the phonon modes coupled with the orbital ordering as well as the orbital excitations in this one-dimensional orbital system. In Fig. 2, we display the Raman scattering spectra at various temperatures in the polarization configurations of $y(zz)\bar{y}$ and $y(xx)\bar{y}$ for $LaVO_3$, $NdVO_3$, and YVO_3 single crystals. The Raman spectra for the polarization configurations of $y(zx)\bar{y}$, $y'(x'x')\bar{y}'$, $z(x'y')\bar{z}$, and $z(xy)\bar{z}$ were also measured, where $x+y=x'$ and $x-y=y'$. No additional electronic Raman band is discerned in the spectra for these polarizations in the *C*-type spin- and *G*-type orbital-ordered phase except for the originally active phonon modes. First,

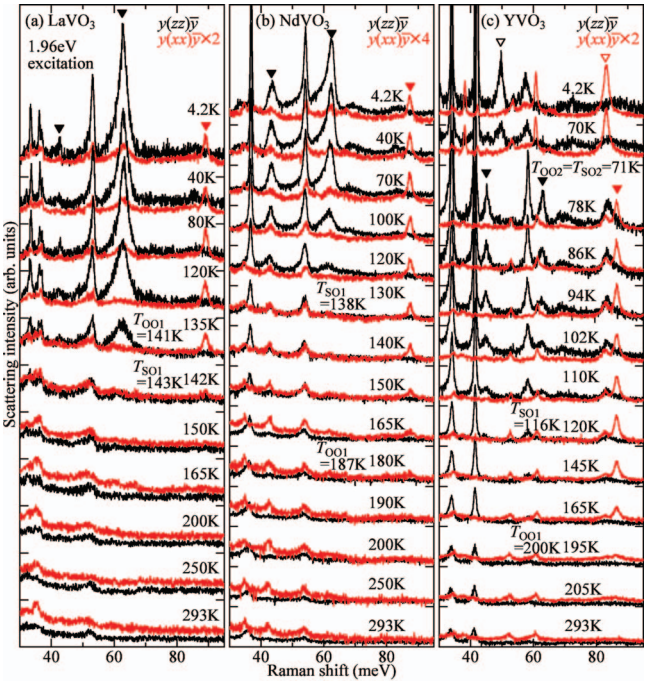

FIG. 2. (Color) Raman scattering spectra for the polarization configurations of $y(zz)\bar{y}$ and $y(xx)\bar{y}$ at various temperatures in (a) $LaVO_3$, (b) $NdVO_3$, and (c) YVO_3 with the exciting photon energy of 1.96 eV. The 43 and 62 meV peaks in $y(zz)\bar{y}$ polarization in the *C*-type spin- and *G*-type orbital-ordered phase, indicated by the filled black triangles, are assigned to the two-orbiton excitation of highly one-dimensional character, while those between 85 and 90 meV in $y(xx)\bar{y}$ polarization, by a closed red triangle, to the phonon mode observed in the *G*-type orbital-ordered phase. Here, T_{OO1}, T_{SO1}, and $T_{SO2}(=T_{OO2})$ are the transition temperatures of the *G*-type orbital ordering, the *C*-type spin ordering, and the *G*-type spin and *C*-type orbital ordering, respectively. Other peak structures appear in the *G*-type spin- and *C*-type orbital-ordered phase in YVO_3 ($T<T_{SO2}$). The 50 meV band in $y(zz)\bar{y}$ polarization, indicated by an open black triangle, has magnetic origin, while the 83 meV one in $y(xx)\bar{y}$ polarization, by an open red triangle, are assigned to the phonon mode in this spin- and orbital-ordered state (see text).

we briefly discuss the phonon modes activated by the *G*-type OO. At room temperature, several phonon modes are observed in the $y(zz)\bar{y}$ spectra in RVO_3 (*R*=La, Nd, and Y). The Raman bands around 35 and 53 meV in $LaVO_3$, around 37 and 54 meV in $NdVO_3$, and around 41 and 58 meV in YVO_3 are assigned to oxygen bending and Jahn-Teller modes, respectively. In YVO_3, another phonon mode related with the rotation of the VO_6 octahedra is also observed around 34 meV. The phonon mode of the same origin appears around 23 meV in $LaVO_3$ and around 27 meV in $NdVO_3$ (see Fig. 4). As the ionic size of *R* is decreased from La to Y in RVO_3, the orthorhombic distortion, which shows the same tilting habit of VO_6 octahedra as the collective Jahn-Teller one coupled with the *G*-type orbital ordering, increases gradually. The decrease of the V-O-V bond angle and increase of the Jahn-Teller distortion cause the systematic enhancement and shift of the oxygen bending and Jahn-Teller modes. As temperature is decreased, additional peaks due to oxygen stretching mode, which are indicated by

closed red triangles in Fig. 2, appear at 89 meV in $LaVO_3$, at 87 meV in $NdVO_3$, and at 86 meV in YVO_3 below T_{OO1} (=141, 187, and 200 K, respectively) in the polarization configuration of $y(xx)\bar{y}$. These phonon modes are observed also in the $z(x'y')\bar{z}$ spectra. According to the factor group analysis, the *Pbnm* orthorhombic symmetry in RVO_3 at room temperature allows 24 Raman active modes, $7A_g+5B_{1g}+7B_{2g}+5B_{3g}$. In the temperature region of $T<T_{OO1}$, the *Pbnm* orthorhombic lattice symmetry is lowered into the $P2_1/a$ monoclinic form in RVO_3, and the phonon modes are mixed up and sorted into A_g and B_g representations $7A_g+5B_{1g} \rightarrow 12A_g$ and $7B_{2g}+5B_{3g} \rightarrow 12B_g$.[8,13,14,21–23] Below T_{OO1}, all the phonon modes in $y(zz)\bar{y}$ and $y(xx)\bar{y}$ configurations have the A_g symmetry. The Raman bands between 85 and 90 meV in the polarization configuration of $y(xx)\bar{y}$, which have the B_{1g} symmetry in the original *Pbnm* lattice, appear only in the monoclinic phase coupled with the *G*-type OO.[8]

Among these three compounds, YVO_3 undergoes the second spin- and orbital-ordering transition at $T_{SO2}=T_{OO2}=71$ K, as temperature is lowered. This magnetic and orbital transition is accompanied by the structural change from the intermediate-temperature monoclinic phase to the lowest-temperature orthorhombic one with *Pbnm* symmetry.[8,11–13] In the intermediate-temperature region of $T_{SO2}=T_{OO2}<T<T_{OO1}$, the Raman spectra in the polarization configuration of $y(xx)\bar{y}$ in YVO_3 have two peaks around 85 meV.[24] In the *G*-type orbital-ordered phase, the intensity of the higher-lying peak at 86 meV is larger than that of the lower-lying one at 83 meV. As shown in Figs. 2(c) and 3(c), the higher-lying 86 meV phonon mode disappears below T_{SO2}, while the lower-lying 83 meV one survives and its intensity is remarkably enhanced. The 86 and 83 meV Raman bands in YVO_3 are related closely with the intermediate-temperature monoclinic structure accompanied by the *G*-type OO, and with the low-temperature orthorhombic one coupled with the *C*-type OO, respectively. In the next session (Sec. IV), the two-peak feature in the intermediate-temperature phase of YVO_3 are discussed in detail. The band around 50 meV in the $y(zz)\bar{y}$ spectra below T_{SO2} [indicated by an open triangle in Fig. 2(c)] is also explained in Sec. IV.

In the *C*-type spin- and *G*-type orbital-ordered phase, new bands emerge around 43 and 62 meV in the polarization configuration of $y(zz)\bar{y}$, as indicated by closed black triangles in Fig. 2. Below T_{OO1}, the 43 and 62 meV peaks in $y(zz)\bar{y}$ polarization appear in $LaVO_3$, where the magnetic transition occurs right above T_{OO1} ($T_{SO1}=143$ K in $LaVO_3$). On the other hand, these peaks are discerned only below T_{SO1}(=138 and 116 K, respectively) in $NdVO_3$ and YVO_3, which undergo the *G*-type OO far above T_{SO1}. We assign these bands to the orbital excitations on the basis of the following arguments. (As for the general difficulty to distinguish the orbital excitation and multiphonon mode, see also the controversy reported by the papers in Ref. 6.)

First, width of the peaks is much broader than those of the single $k=0$ phonons, and additionally the 62 meV band has a distinctly asymmetric shape. As for the 62 meV band, any plausible combinations of the lower-lying Raman and infrared phonon modes cannot account for its Raman shift, which excludes a possibility of two- (or multi)phonon excitation as

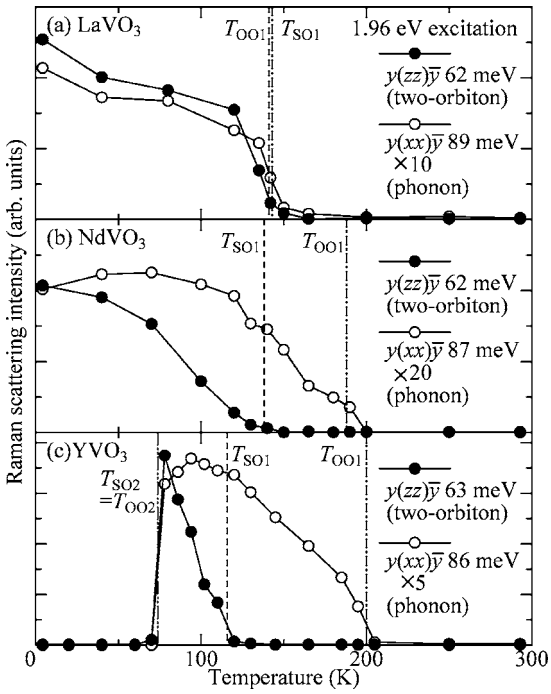

FIG. 3. Temperature dependence of the integrated Raman scattering intensity of the peak around 62–63 meV in the polarization configuration of $y(zz)\bar{y}$ (closed circles) and that around 86–89 meV in $y(xx)\bar{y}$ (open circles) for (a) $LaVO_3$, (b) $NdVO_3$, and (c) YVO_3. The peak structures in the polarization configuration of $y(zz)\bar{y}$ are assigned to the two-orbiton excitations, while those in $y(xx)\bar{y}$ to the phonon modes. Vertical broken, dash-dotted, and double-dash-dotted lines indicated the transition temperatures of the *C*-type spin ordering (T_{SO1}), the *G*-type orbital ordering (T_{OO1}), and the *G*-type spin and *C*-type orbital ordering ($T_{SO2}=T_{OO2}$), respectively. Solid lines are the guide to the eyes.

the origin of this Raman band. The peak energy of the 43 meV would not be inconsistent with two-phonon process of the infrared-active external mode (corresponding to rare-earth motion) in $LaVO_3$ and $NdVO_3$. However, such a mode couples most weakly with electronic state of V atoms. It is not reasonable to assume that only the two-phonon band of the rare-earth mode could be sensitively activated only below T_{SO1}. The 43 meV mode is also observed in the *C*-type spin- and *G*-type orbital-ordered state in YVO_3, where twice of the rare-earth mode frequency shows no more coincidence with the 43 meV band.[21] As shown in Fig. 3, the temperature dependence of the band around 62 meV is clearly different from that of the 86–89 meV phonon band that stands for the OO induced lattice distortion. The steep rise of the intensity of the 62 meV band below T_{SO1} indicates that this (as well as 43 meV) band is inherent to the concomitantly *C*-type spin- and *G*-type orbital-ordered state. Moreover, the linewidth of the band around 62 meV critically increases as temperature is increased toward T_{SO1}, whereas those of phonons are almost unchanged apart from conventional thermal broadening.[20] In addition, Raman shifts of phonon increase systematically as the ionic size of *R* is decreased from that of La to Y, while those of the peaks around 43 and 62 meV are almost unchanged. These features imply that these two bands around 43 and 62 meV have a magnetic or electronic origin.

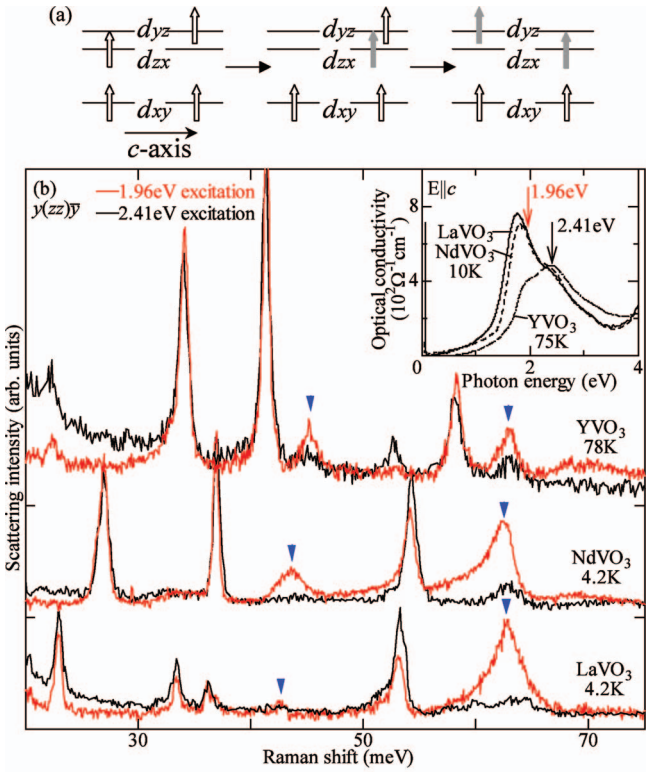

FIG. 4. (Color) (a) Two-orbiton Raman scattering process in the antiferroic (staggered) orbital chain with the ferromagnetic spin order. (b) Raman scattering spectra at 4.2 K in $LaVO_3$ and $NdVO_3$, and that at 78 K in YVO_3 with the exciting photon energies of 1.96 and 2.41 eV. The blue triangles indicate the two-orbiton Raman modes. The inset presents optical conductivity spectra for $\mathbf{E}\|c$ at 10 K in $LaVO_3$ and $NdVO_3$ and that at 75 K in YVO_3.

However, genuine charge excitations cannot be responsible for these bands, because the lowest Mott-Hubbard gap energy is too large ($\sim$2 eV), as described later. On the other hand, magnon excitations are almost gapless and the observed peak energies are too high to ascribe to the single magnon band. Furthermore, in the *C*-type spin-ordered state which has a ferromagnetic order along the *c* axis, two-magnon excitation is prohibited in the polarization configuration of $y(zz)\bar{y}$. In contrast to the almost constant Raman shifts of 43 and 62 meV peaks in $LaVO_3$ and YVO_3, spin-wave dispersion in $LaVO_3$ is quite different from that in YVO_3.[11] The absence of *R* dependence of the Raman shifts around 43 and 62 meV suggests that the Raman bands are not caused by two magnons nor related magnetic excitations in the long-range spin-ordered state. Therefore, we can assign the origin of the Raman bands to orbital excitations. The Jahn-Teller mode at 53–58 meV is discerned from high temperature, and the intensity is enhanced together with the bands around 43 and 62 meV as temperature is lowered. This implies that the Jahn-Teller phonon is coupled with these Raman bands which are assigned to orbital excitations.

To gain further insight into the Raman process related to the orbital excitations, it is important to consider the Mott-Hubbard gap transition as the intermediate state. The inset of Fig. 4(b) presents optical conductivity spectra for $\mathbf{E}\|c$ at 10 K in $LaVO_3$ and $NdVO_3$, and that at 75 K in YVO_3.[18] The Mott-Hubbard gap transition is observed as a distinct peak around 2 eV in this spin- and orbital-ordered phase in RVO_3. The 2 eV band in the optical conductivity spectrum for $\mathbf{E}\|c$ is composed of two peaks. The lower-lying peak around 1.9 eV has been assigned to the orbital-dependent Mott-Hubbard gap transition in the *C*-type spin- and *G*-type orbital-ordered phase.[18] In the photoexcitation process in this phase, an electron can hop only between the d_{zx} orbitals or the d_{yz} ones on the neighboring V sites along the *c* axis through the π bonding with the O $2p_x$ or $2p_y$ state, as shown in the left and middle panels of Fig. 4(a).[16,18] The d_{yz}-d_{yz} transition energy should be nearly equal to the d_{zx}-d_{zx} one.

The broad Raman bands around 43 and 62 meV show a resonance with this Mott-Hubbard gap transition. Figure 4(b) represents a comparison between the Raman scattering spectra at 4.2 K in $LaVO_3$ and $NdVO_3$, and those at 78 K in YVO_3, observed with two exciting photon energies of 1.96 and 2.41 eV. In these compounds, the 43 and 62 meV Raman bands are enhanced, when the exciting photon energy is 1.96 eV, almost equal to the energy of the Mott-Hubbard gap transitions in the *C*-type spin- and *G*-type orbital-ordered state. The resonant enhancement of the 43 and 62 meV Raman bands is conspicuous for $LaVO_3$ and $NdVO_3$, reflecting the sharp peak structure of their optical conductivity spectra at 1.9 eV, while that for YVO_3 is moderate perhaps due to the less-distinct shape of the Mott-Hubbard gap peak around 1.96 eV, as shown in the inset of Fig. 4(b). It is thus reasonable to consider that this resonant Raman process involves the Mott-Hubbard gap transition as the intermediate state [the middle panel of Fig. 4(a)]. In the final state of this Raman process, the orbital occupancy of the adjacent V sites along the *c* axis is exchanged as compared with that of the initial state. We call this elementary excitation two-orbiton by analogy to two-magnon in an antiferromagnetically ordered state.

In the previous study,[20] we have given a theoretical account for the orbital excitation observed in the Raman scattering in terms of the one-dimensional Heisenberg model for orbital pseudospin. The theoretical investigation has demonstrated that the feature of the two-orbiton Raman spectra, such as the Raman shift and spectral shape, are determined by the particle-hole excitation for the pseudospinon band, which is gapped by the Jahn-Teller effect. The observed two Raman bands, around 43 and 62 meV, have been assigned to the lower and upper edges of the particle-hole excitation continuum, respectively, accompanying the van Hove singularities in one dimension. When the ionic radius of the *R*-site ion decreases, the tilting of VO_6 and the Jahn-Teller distortion increase, and the orbital exchange interaction is suppressed. The lower-lying Raman orbiton peak around 43 meV slightly increases in its shift, while sharpening the band shape, with the change of the *R*-site ion from La to Y. These spectral features can be explained by the change of the energies of the exchange interaction and Jahn-Teller effect. As for the lower-lying peak around 43 meV, the scattering intensity should be enhanced and its shift increased by the increase of the Jahn-Teller distortion, as observed and predicted.[20,25,26] At the present stage, however, we cannot exclude the possibility of the one-orbiton excitation for this lower-lying band. The increase of the tilting of the VO_6 octahedra modifies the

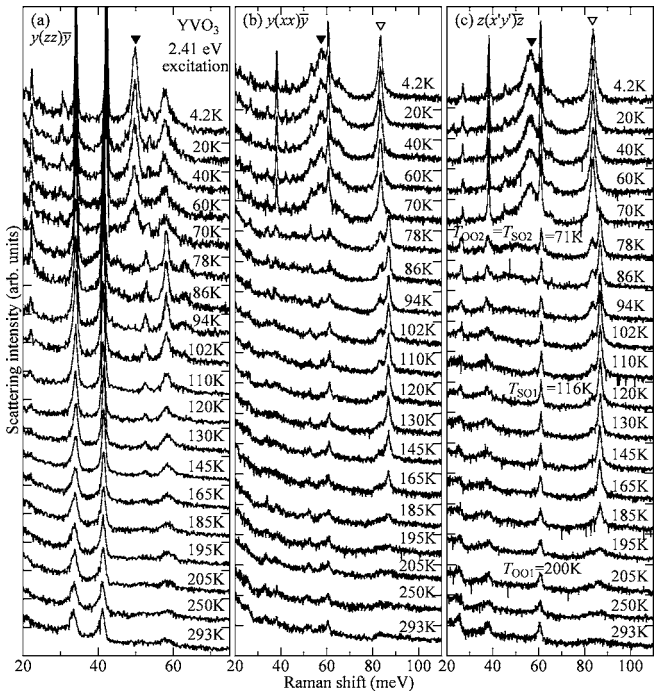

FIG. 5. Raman scattering spectra for the polarization configurations of (a) $y(zz)\bar{y}$, (b) $y(xx)\bar{y}$, and (c) $z(x'y')\bar{z}$ at various temperatures in YVO_3 with the exciting photon energy of 2.41 eV. The open triangles indicate the oxygen stretching phonon mode in the *G*-type spin- and *C*-type orbital-ordered phase. Below the second magnetic transition temperature (=71 K), three broad Raman bands emerge around 50 meV in the polarization configuration of $y(zz)\bar{y}$, and around 57 meV in $y(xx)\bar{y}$ and $z(x'y')\bar{z}$ polarizations, which are indicated by closed triangles.

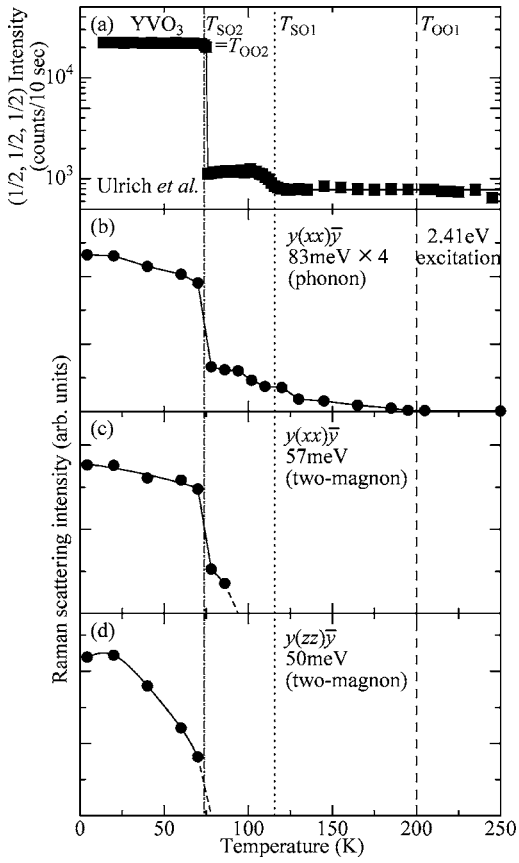

FIG. 6. Temperature-dependent intensity of the magnetic (1/2, 1/2, 1/2) reflection reported by Ulrich *et al.* (Refs. 11 and 27) is shown in the top panel (a). (b) Temperature dependence of the integrated Raman scattering intensity of the peak around 83 meV in the polarization configuration of $y(xx)\bar{y}$ assigned to phonon, (c) that around 57 meV in $y(xx)\bar{y}$ polarization to two-magnon, and (d) that around 50 meV in $y(zz)\bar{y}$ polarization to two-magnon in YVO_3. Vertical broken, dotted, and dash-dotted lines indicate the transition temperatures of the *G*-type orbital ordering (T_{OO1}), the *C*-type spin ordering (T_{SO1}), and the *G*-type spin *C*-type orbital ordering ($T_{SO2}=T_{OO2}$), respectively. Solid lines are the guide to the eyes.

selection rule and allows the interorbital transition on the neighboring V sites along the *c* axis. Consequently, the one-orbiton might be observed by the Raman scattering spectroscopy.

IV. *G*-TYPE SPIN- AND *C*-TYPE ORBITAL-ORDERED PHASE

YVO_3 is known to undergo the second magnetic and orbital transition from the higher-temperature *C*-type spin- and *G*-type orbital-ordered state to the lower-temperature *G*-type spin- and *C*-type orbital-ordered one.[10–13] In this section, we show the results of Raman scattering spectroscopy, and discuss the activated phonon and the magnetic excitation in the *G*-type spin- and *C*-type orbital-ordered phase of YVO_3. In Fig. 5, we display the Raman scattering spectra with the polarization configurations of $y(zz)\bar{y}$, $y(xx)\bar{y}$, and $z(x'y')\bar{z}$ at various temperatures in YVO_3 by utilizing the Ar ion laser 514.5 nm (2.41 eV) line as an exciting light. First, we discuss the Raman phonon band coupled with the *C*-type OO. As shown in Figs. 5(b) and 5(c), the phonon band assigned to the oxygen stretching mode is observed at 83 meV (indicated by the open triangles) in the polarization configurations of $y(xx)\bar{y}$ and $z(x'y')\bar{z}$ at the ground state. This 83 meV phonon mode has the B_{1g} symmetry in the lowest-temperature orthorhombic *Pbnm* lattice. As temperature is increased, the intensity of the 83 meV band is suppressed above T_{SO2} ($=T_{OO2}=71$ K), but survives even in the *G*-type orbital-ordered phase [see Figs. 5(b), 5(c), and 6(b)]. Between $T_{OO2}=T_{SO2}$ and T_{OO1}(=200 K), the additional Raman band appears at 86 meV. In this intermediate temperature region, the intensity of the 83 meV is lower than that of the 86 meV one. With further increase of temperature, the 83 meV phonon band rapidly decays above T_{SO1}(=116 K), while the 86 meV band is clearly observed in the higher-temperature *G*-type orbital-ordered phase up to T_{OO1}(=200 K), as described in the previous section. The temperature-dependent behavior of these phonon Raman bands at 83 and 86 meV remains unchanged even when the exciting photon energy is changed from 2.41 to 1.96 eV.

The 83 meV phonon band is distinctly observed in the lowest-temperature orthorhombic phase coupled with the *C*-type orbital-ordered state, while the 86 meV one appears only in the *G*-type orbital-ordered phase. This result indicates that the 83 and 86 meV phonon modes couple with the

respective OO patterns. Between T_{SO2} and T_{OO1}, such a two-peak feature of phonon mode implies the coexistence or mixture of two types of OO or related lattice distortion in the nominally *G*-type OO phase in YVO_3. [Note that the OO-induced phonon mode (~85 meV) shows no splitting for the *G*-type OO phase of $LaVO_3$ and $NdVO_3$.] In contrast, the simple phonon band around 40 meV in the $y(zz)\bar{y}$ polarization shows a single-peak feature in the whole temperature region, while the Raman shift of this phonon band changes from 41 to 42 meV at T_{SO2}. The results exclude the possibility that the monoclinic structure coupled with the long-range *G*-type orbital-ordered phase may coexist with the orthorhombic one in the *C*-type orbital-ordered phase between T_{SO2} and T_{OO1}. Therefore, the two-peak feature around 85 meV phonon bands at $T_{SO2}<T<T_{OO1}$ suggests the existence of the large fluctuation or short-range correlation of the *C*-type OO mixed in the nominally *G*-type OO. In the investigation of neutron scattering, Ulrich *et al.* have observed the (1/2, 1/2, 1/2) Bragg reflection in the *C*-type antiferromagnetic phase, most of whose intensity is of magnetic origin.[27] We plot the temperature-dependent intensity of the magnetic (1/2, 1/2, 1/2) Bragg reflection in Fig. 6(a). The existence of the reflection (1/2, 1/2, 1/2) suggests that the *G*-type magnetic components survive even in the temperature region of $T_{SO2}<T<T_{SO1}$, i.e., in the *C*-type spin-ordered phase. Again, there is observed no phase-coexistence nor phase-separation feature in the static averaged lattice structure.[11] The present Raman scattering study implies that the *C*-type orbital order or correlation exists as the source of the *G*-type magnetic component in the nominally *C*-type magnetic and *G*-type orbital-ordered phase of YVO_3. Thus, the OO and SO may be complex between T_{OO1} and T_{OO2} in YVO_3. This is perhaps because YVO_3 is located on the verge of the boundary between the two types of orbital- and spin-ordered phases, where the large fluctuation or short-range correlation of spin and orbital exists. In contrast, the pattern of the orbital is simple *G* type in other compounds such as $LaVO_3$ and $NdVO_3$, which are far away from the phase boundary of these two spin- and orbital-ordered states in the phase diagram. At the present stage, however, we do not have any more explicit scenario to elucidate the complicated behavior of spin and orbital in YVO_3. This puzzling orbital dynamics would deserve further experimental and theoretical investigations.

As shown in Figs. 5, 6(c) and 6(d), the Raman band around 50 meV in the $y(zz)\bar{y}$ polarization, and the bands around 57 meV in the $y(xx)\bar{y}$ and $z(x'y')\bar{z}$ ones (indicated by the closed triangles) emerge below T_{SO2}, i.e., in the *G*-type spin- and *C*-type orbital-ordered phase. The 57 meV bands are common for the polarization configurations of $y(xx)\bar{y}$ and $z(x'y')\bar{z}$ and hence has the B_{1g} symmetry in the *Pbnm* lattice, while the 50 meV band in the $y(zz)\bar{y}$ polarization has the A_g symmetry. These Raman bands are much broader in shape than conventional phonon modes. The broad bandwidth feature would suggest that the Raman bands might be assigned to the two- (or multi)phonon mode, but no possible combinations of the lower-lying phonon modes can explain the positions of these broad bands. Moreover, the Raman bands around 50 and 57 meV are observed only in the lowest-temperature *G*-type spin- and *C*-type orbital-ordered phase, where the lattice symmetry (*Pbnm*) is the same as that in the high-temperature spin- and orbital-disordered phase. Above T_{OO1}, no corresponding phonon modes are observed around 50 meV in the $y(zz)\bar{y}$ spectrum and around 57 meV in the $y(xx)\bar{y}$ and $z(x'y')\bar{z}$ ones. These features indicate that these Raman bands are assigned to a magnetic or electronic excitation mode coupled with the *G*-type SO and *C*-type OO. However, the assignment to the charge excitation also seems unlikely, because the observed frequency of these peaks at the lowest temperature is even less than the charge-gap energy (~2 eV) proved by optical conductivity spectra [the insets of Figs. 4(b) and 7]. The antiferromagnetic arrangement of the V^{3+} spins in all three directions tends to prevent the genuine orbital excitations in the lowest-temperature phase in YVO_3, in contrast to the *C*-type spin-ordered one. Therefore, we assigned these two peaks to the two-magnon scattering, where one photon ($k\sim0$) excites two magnons with the wave vectors k and $-k$ simultaneously.[28,29] As for the B_{1g} mode around 57 meV, the scattering intensity is rapidly suppressed around T_{SO2}. Nevertheless, the bands survive even above T_{SO2}, although not only softened but also severely broadened [Figs. 5(b) and 5(c)]. As mentioned above, the previous study of the neutron scattering has indicated that the *G*-type antiferromagnetic component exists above T_{SO2}.[11] This is in accord with the subsistence of the B_{1g} two-magnon mode above T_{SO2}.

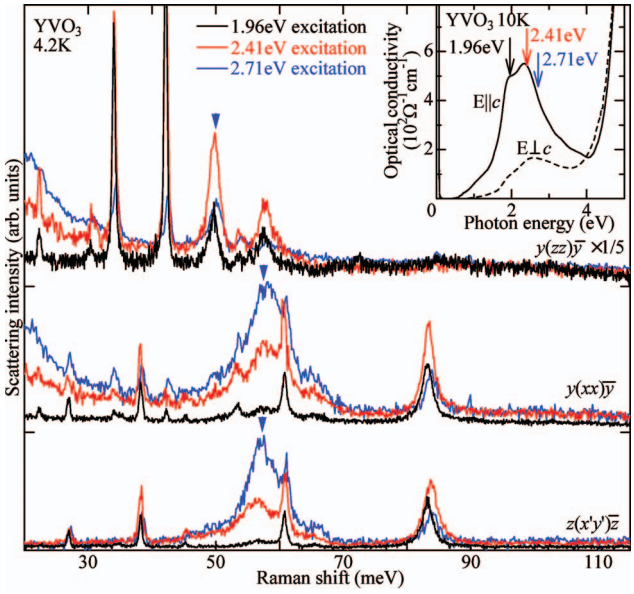

FIG. 7. (Color) Raman scattering spectra at 4.2 K in YVO_3 with the exciting photon energies of 1.96, 2.41, and 2.71 eV. The blue triangles indicate the peak structures due to the two-magnon Raman modes. The inset presents optical conductivity spectra for $\mathbf{E}\|c$ and $\mathbf{E}\perp c$ at 10 K in YVO_3.

To gain a further insight into the spectral feature of the two-magnon bands, the resonance effect of Raman scattering has been investigated. Figure 7 represents a comparison between the Raman scattering spectra at 4.2 K (in the *G*-type spin- and *C*-type orbital-ordered phase) in YVO_3, observed with three exciting photon energies of 1.96, 2.41, and

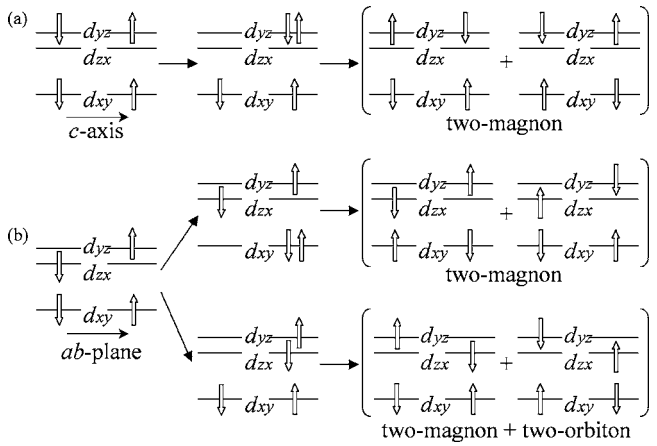

FIG. 8. Possible resonant Raman scattering process with the Mott-Hubbard gap transitions as the intermediate state in the *G*-type spin- and *C*-type orbital-ordered state. The two configurations in the final state (right row) constitute the local $m_s=0$ states.

2.71 eV. The 50 meV Raman band in the polarization configuration of $y(zz)\bar{y}$ in YVO_3 is enhanced, when the exciting photon energy is 2.41 eV. As shown in the inset of Fig. 7, the optical conductivity spectrum for $\mathbf{E}\|c$ has a peak structure around 2.41 eV, which is assigned to the d_{yz}-d_{yz} or d_{zx}-d_{zx} transition between the neighboring V sites along the *c* axis through the π bonding with the O $2p_y$ or $2p_x$ state in this *G*-type spin- and *C*-type orbital-ordered phase.[18] The resonant feature of Raman scattering indicates that the Raman process involves the orbital-dependent Mott-Hubbard gap transition as the intermediate state. Figure 8(a) represents the possible Raman processes, which include the Mott-Hubbard gap transition as one of the intermediate states. By the interaction with the photon, the d_{yz} (d_{zx}) electrons can resonantly return to the neighboring V site along the *c* axis. In the final state of this Raman process, the spins, but not the orbitals, of the adjacent V sites along the *c* axis is exchanged as compared with that of the initial state. [The two configurations shown as the final state in Fig. 8(a) are quantum-mechanically indistinguishable in this local representation, constituting the local $m_s=0$ states.]

On the other hand, the 57 meV Raman band in the $y(xx)\bar{y}$ and $z(x'y')\bar{z}$ polarizations shows a different behavior of the resonance effect from that of the 50 meV one in the $y(zz)\bar{y}$ in YVO_3. As shown in Fig. 7, the scattering intensity of the 57 meV band monotonously increases, when the exciting photon energy increases from 1.96 to 2.71 eV. The optical conductivity spectrum for $\mathbf{E}\perp c$ has a broad peak due to Mott-Hubbard gap transition around 2.6 eV. The observed resonant feature suggests that the Raman process may involve the Mott-Hubbard gap transitions between the neighboring V sites in the *ab* plane, or alternately or concurrently the charge-transfer gap transition from O $2p$ orbital to V $3d$ one located above 4 eV. Figure 8(b) shows the possible Raman processes for the 57 meV Raman bands. In the *ab* plane, the genuine two-magnon excitation due to the spin exchange between the adjacent d_{xy} states is possible with the optically allowed d_{xy}-d_{xy} transition between the nearest-neighbor V sites [the upper route shown in Fig. 8(b)] as the intermediate state. Another spin exchange process may occur via the adjacent d_{yz}/d_{zx} states [the lower route shown in Fig. 8(b)]. In this resonant process, however, not only the spin but also the occupancy of the orbital are exchanged in the final state, i.e., the two-orbiton plus two-magnon excitation occurs. However, the two-magnon plus two-orbiton mode costs much higher excitation energy, perhaps by a factor of ≈ 2, than that of the two-magnon one. As described below, the excitation energies of these Raman modes seem to be consistent with the spin exchange interaction energies estimated by the neutron scattering study.[11] It is thus likely that the B_{1g} mode around 57 meV is the genuine two-magnon excitation in origin, but not the two-magnon plus two-orbiton one.

By the neutron scattering study on the spin wave dispersion in the *G*-type spin-ordered state of YVO_3, Ulrich *et al.*[11] have deduced the spin exchange interaction parameters, $J \sim J_{ab} \sim J_c \sim 5.7 \pm 0.3$ meV on the basis of $S=1$ anisotropic Heisenberg model. In the classical limit of the *G*-type spin order, a pair of spin excitations on the neighboring sites costs the energy of $2(z-1)JS=10JS$, *z* being the number of the nearest neighbors. A more elaborate estimate on the Raman two-magnon peak energy $\Omega_{2\text{-mag}}$ in the *G*-type antiferromagnet with $S=1$ has been reported for NiO ($S=1$); $\Omega_{2\text{-mag}} = 10.2J$.[30] With use of the $J=5.7$ meV, the $\Omega_{2\text{-mag}}$ for the *G*-type spin ordered state of YVO_3 is estimated to be 58 meV. This value is in good agreement with the observed Raman shifts ($\sim$50 and $\sim$57 meV) which were assigned here to the two-magnon excitations.

V. SUMMARY

Lattice, magnetic and orbital excitations have been investigated in the t_{2g} electron system, RVO_3 (R=La, Nd, and Y), by measurements of the polarized and resonant Raman scattering spectra. In this system, the phonons, which distinctly couple with the respective orbital-ordered states, i.e., *G*-type and *C*-type, are observed between 85 and 90 meV in the $y(xx)\bar{y}$ and $z(x'y')\bar{z}$ Raman spectra. These phonon modes have B_{1g} symmetry in the original *Pbnm* lattice at room temperature. A single peak constitutes this phonon band in the simple *G*-type orbital-ordered phase in $LaVO_3$ and $NdVO_3$. In contrast, the phonon band shows a two-peak feature in the intermediate-temperature *G*-type orbital-ordered phase in YVO_3, reflecting the existence of the short-range correlation or fluctuation of orbital *C* type. In YVO_3, the two-magnon excitations are observed in the low-temperature *G*-type antiferromagnetic phase. The Raman shifts of the two-magnons are consistent with the magnon dispersion revealed by neutron scattering study.[11] In all the RVO_3 compounds, orbital excitation bands have been observed in the $y(zz)\bar{y}$ spectra in the *C*-type spin- and *G*-type orbital-ordered phase. The temperature and *R* dependence and the resonant effect of the Raman spectra have indicated that the orbital excitation bands are distinguished from other excitations and assigned to a two orbiton, which exchanges the occupancy of yz/zx orbitals on the nearest-neighbor V site along the *c* axis.

ACKNOWLEDGMENTS

We would like to thank S. Onoda, N. Nagaosa, S. Ishi-

hara, Y. Motome, and B. Keimer for helpful discussions. This work was supported by KAKENHI (Grant Nos. 16740192, 17340104, 15104006) and TOKUTEI (Grant No. 16076205) from JPSJ and MEXT.

[1] N. F. Mott, *Metal-Insulator Transitions* (Taylor and Francis, London, 1990).
[2] M. Imada, A. Fujimori, and Y. Tokura, Rev. Mod. Phys. **70**, 1039 (1998).
[3] *Physical Properties of High Temperature Superconductors*, edited by D. M. Ginzburg (World Scientific, Singapore, 1992), Vol. 3.
[4] *Colossal Magnetoresistive Oxides, Vol. 2 of Advances in Condensed Matter Science*, edited by Y. Tokura (Gordon and Breach, Amsterdam, 2000).
[5] Y. Tokura and N. Nagaosa, Science **228**, 462 (2000).
[6] E. Saitoh, S. Okamoto, K. T. Takahashi, K. Tobe, K. Yamamoto, T. Kimura, S. Ishihara, S. Maekawa, and Y. Tokura, Nature (London) **410**, 180 (2001). Concerning the controversy about the orbiton interpretation, see also M. Grüninger, R. Rückamp, M. Windt, P. Reutler, C. Zobel, T. Lorenz, A. Freimuth, and A. Revcolevschi, *ibid.* **418**, 39 (2002); and E. Saitoh, S. Okamoto, K. Tobe, K. Yamamoto, T. Kimura, S. Ishihara, S. Maekawa, and Y. Tokura, *ibid.* **418**, 40 (2002).
[7] B. Keimer, D. Casa, A. Ivanov, J. W. Lynn, M. v. Zimmermann, J. P. Hill, D. Gibbs, Y. Taguchi, and Y. Tokura, Phys. Rev. Lett. **85**, 3946 (2000).
[8] S. Miyasaka, Y. Okimoto, M. Iwama, and Y. Tokura, Phys. Rev. B **68**, 100406(R) (2003).
[9] V. G. Zubkov, G. V. Bazuev, and G. P. Shveikin, Sov. Phys. Solid State **15**, 1079 (1973).
[10] H. Kawano, H. Yoshizawa, and Y. Ueda, J. Phys. Soc. Jpn. **63**, 2857 (1994).
[11] C. Ulrich, G. Khaliullin, J. Sirker, M. Reehuis, M. Ohl, S. Miyasaka, Y. Tokura, and B. Keimer, Phys. Rev. Lett. **91**, 257202 (2003).
[12] M. Noguchi, A. Nakazawa, S. Oka, T. Arima, Y. Wakabayashi, H. Nakao, and Y. Murakami, Phys. Rev. B **62**, R9271 (2000).
[13] G. R. Blake, T. T. M. Palstra, Y. Ren, A. A. Nugroho, and A. A. Menovsky, Phys. Rev. Lett. **87**, 245501 (2001).
[14] P. Bordet, C. Chailout, M. Marezio, Q. Huang, A. Santoro, S-W. Cheong, H. Takagi, C. S. Oglesby, and B. Batlog, J. Solid State Chem. **106**, 253 (1993).
[15] Y. Ren, T. T. M. Palstra, D. I. Khomskii, E. Pellegrin, A. A. Nugroho, A. A. Menovsky, and G. A. Sawatzky, Nature (London) **396**, 441 (1998).
[16] Y. Motome, H. Seo, Z. Fang, and N. Nagaosa, Phys. Rev. Lett. **90**, 146602 (2003).
[17] G. Khaliullin, P. Horsch, and A. M. Oleś, Phys. Rev. Lett. **86**, 3879 (2001).
[18] S. Miyasaka, Y. Okimoto, and Y. Tokura, J. Phys. Soc. Jpn. **71**, 2086 (2002).
[19] S. Ishihara, Phys. Rev. B **69**, 075118 (2004).
[20] S. Miyasaka, S. Onoda, Y. Okimoto, J. Fujioka, M. Iwana, N. Nagaosa, and Y. Tokura, Phys. Rev. Lett. **94**, 076405 (2005).
[21] A. A. Tsvetkov, F. P. Mena, P. H. M. van Loosdrecht, D. van der Marel, Y. Ren, A. A. Nugroho, A. A. Menovsky, I. S. Elfimov, and G. A. Sawatzky, Phys. Rev. B **69**, 075110 (2004).
[22] Recently, Tsvetkov *et al.* have proposed other structure for the *G*-type orbital-ordered phase in YVO_3, which has a monoclinic $Pb11$ or a triclinic $P\bar{1}$ (Ref. 21). These structures are a subgroup of the *Pbnm* symmetry. In the $P\bar{1}$ triclinic structure, all the Raman phonons have A_g symmetry, while the Raman phonons are mixed up with the infrared ones in the $Pb11$ monoclinic one. However, the structural feature and the pattern of the orbital ordering are still controversial for RVO_3, in particular for YVO_3. The orbital Peierls state with bond dimerization has also been proposed for YVO_3 (Refs. 11 and 23).
[23] P. Horsch, G. Khaliullin, and A. M. Oleś, Phys. Rev. Lett. **91**, 257203 (2003).
[24] The spectral shape around 85 meV in the present study, i.e., two-peak structure, is different from that reported in Ref. 8. In the previous investigation, the YVO_3 crystal was not correctly oriented. Perhaps, the Raman spectra in Fig. 3(a) in Ref. 8 were dominated by the polarization configuration of $y(zz)\bar{y}$. As for the Raman band around 85 meV in the $y(zz)\bar{y}$ polarization, the broad shape and the temperature dependence imply that this mode may be electronic in origin, closely related with the spin- and orbital-ordered state. In the lightly hole-doped systems, $La_{1-x}Sr_xVO_3$, $Nd_{1-x}Sr_xVO_3$, and $Pr_{1-x}Ca_xVO_3$ ($0<x<0.1$), the same Raman mode is observed in the *C*-type spin- and *G*-type orbital-ordered state. This mode seems to emerge, when the selection rule in the *C*-type spin- and *G*-type orbital-ordered state is modified by the hole doping or the *G*-type magnetic component accompanied perhaps by the *C*-type orbital one (Ref. 11).
[25] Recently, Sugai and Hirota have reported the Raman scattering study for YVO_3 (Ref. 26). The experimental result in Ref. 26 is in accord with the present one. However, their assignment of the orbiton band is different from ours.
[26] S. Sugai and K. Hirota, Phys. Rev. B **73**, 020409(R) (2006).
[27] In Ref. 11, Ulrich *et al.* have indexed the reciprocal lattice in terms of a pseudocubic subcell with lattice parameters $a/\sqrt{2}$, $b/\sqrt{2}$, and $c/2$.
[28] P. A. Fleury and R. Loudon, Phys. Rev. **166**, 514 (1968).
[29] S. R. Chinn, H. J. Zeiger, and J. R. O'Connor, Phys. Rev. B **3**, 1709 (1971).
[30] M. J. Massey, N. H. Chen, J. W. Allen, and R. Merlin, Phys. Rev. B **42**, 8776 (1990).